UDC 621.313.33 https://doi.org/10.20998/2074-272X.2025.2.02

V.I. Milykh

Numerical-field analysis of differential leakage reactance of stator winding in three-phase induction motors

Introduction. *The differential leakage reactance (DLR) of the stator winding of three-phase induction motors (TIM) is considered. It is known that DLR is the sum of the self-induction resistances of the winding from all harmonics of its magnetic field, excluding the first one, and its analytical definition is too complicated. But this reactance is a mandatory design element, including for calculating a number of other parameters and characteristics of such motors.* ***Problem.*** *Because of this, in the current classical design methods, the DLR are determined by a simplified formula with the addition of a number of coefficients, tabular and graphical dependencies. As a result, not only the physical and mathematical meaning of DLR is lost, but even the accuracy of its calculation is difficult to assess.* ***Goal.*** *The purpose of the paper consists in the comparative verification of the classical design calculation of the DLR of the TIM stator winding by numerical-field analysis of the harmonic composition of the EMF of self-inductions in this winding and by the determination of the considered DLR on such a basis.* ***Methodology.*** *Harmonic analysis is performed by obtaining the angular and time discrete functions of the magnetic flux linkage (MFL) of the stator winding with their formation in two ways: single-position calculation of the magnetic field and conditional rotation of the phase zones of the winding, or multi-position calculations of the rotating magnetic field and determination of the MFL of stationary phase zones.* ***Results.*** *Computational analysis is performed for nine common variants of TIM, designed according to a single classical method with variation of their power and the number of poles.* ***Originality.*** *A comparison of the results of the classical and numerical-field calculations of the DLR using the FEMM program showed their large discrepancy, which is attributed to the indicated inadequacy of the first one, since the second option is devoid of the shortcomings of the first one due to the fact that it takes into account the dimensions of the TIM structures, the saturation of the magnetic circuit and the physical and mathematical essence of the parameters and values under consideration.* ***Practical value.*** *The presented method of numerical-field analysis and the obtained results of calculating the DLR of the TIM stator winding are recommended as a basis for improving the system of their design. At the same time, a similar approach can be applied to the DLR of the TIM rotor winding, but taking into account its features.* References 27, tables 13, figures 7.

Key words **induction motor, three-phase stator winding, differential leakage reactance, classical design, numerical-field calculations, magnetic flux linkage, harmonic analysis**

Вступ. *Розглядається диференціальний реактивний опір розсіювання (ДРОР) обмотки статора трифазних асинхронних двигунів (ТАД). Відомо, що ДРОР є сумою опорів самоіндукції обмотки від усіх гармонік її магнітного поля за виключенням першої і його аналітичне визначення є надто складним. Але цей опір є обов'язковим елементом проєктування, в тому числі для розрахунку низки інших параметрів та характеристик таких двигунів.* ***Проблема.*** *Через це в чинних класичних методиках проєктування ДРОР визначаються за спрощеною формулою з додаванням низки коефіцієнтів, табличних і графічних залежностей. У підсумку не тільки втрачається фізико-математичний сенс ДРОР, але навіть точність його розрахунку оцінити важко.* ***Мета*** *роботи полягає у порівняльній перевірці класичного проєктного розрахунку ДРОР обмотки статора ТАД шляхом чисельно-польового аналізу гармонічного складу ЕРС самоіндукцій в цій обмотці і визначення на такій основі ДРОР, що розглядається.* ***Методика.*** *Гармонічний аналіз відбувається за отриманням кутових та часових дискретних функцій магнітного потокозчеплення (МПЗ) обмотки статора з їхнім формуванням двома способами: однопозиційним розрахунком магнітного поля і умовним обертанням фазних зон обмотки, або багатопозиційними розрахунками обертового магнітного поля і визначенням МПЗ нерухомих фазних зон.* ***Результати.*** *Розрахунковий аналіз виконано для дев'яті поширених варіантів ТАД, запроєктованих за єдиною класичною методикою з варіюванням їхньої потужності та кількості полюсів.* ***Оригінальність.*** *Порівняння результатів класичного і чисельно-польового розрахунків ДРОР за програмою FEMM показало їхню велику розбіжність, що віднесено до зазначених умовностей і припущень першого, тому що другий варіант позбавлений недоліків першого завдяки тому, що він враховує розміри конструкцій ТАД, насичення магнітопроводу і фізико-математичну сутність параметрів і величин, що розглядаються.* ***Практична цінність.*** *Надана методика чисельно-польового аналізу і отримані результати розрахунку ДРОР обмотки статора ТАД рекомендуються як основа для удосконалення системи їхнього проєктування. При цьому аналогічний підхід можна застосувати і для ДРОР обмотки ротора ТАД, але з урахуванням її особливостей.* Бібл. 27, табл. 13, рис. 7.

Ключові слова: **асинхронний двигун, трифазна обмотка статора, диференціальний реактивний опір розсіювання, класичне проєктування, чисельно-польові розрахунки, магнітне потокозчеплення, гармонічний аналіз.**

Introduction. Three-phase induction motors (TIMs) are diverse and widespread in the technosphere around the world. Their improvement is always relevant and occurs due to various factors, including increasing the accuracy and efficiency of the design system.

Among the design parameters of the TIMs, the active and reactive resistances of its windings are mandatory and important. At the same time, calculations of the inductive resistances of their scattering are usually more complex and insufficiently adequate. This applies to the resistances of differential, slot and frontal scattering, for which specific magnetic conductivities are determined, but in classical design, for example in [1, 2], this is done using methods with fairly approximate formulas.

First of all, this is characteristic of the differential leakage reactance (DLR), which reflects the presence of higher harmonic components in the magnetic field in the gap between the stator and rotor cores. This reactance is determined by a simplified empirical formula that takes into account the minimum parameters of specific TIMs and does not affect the physical essence of the harmonic composition of the specified fields, but it is reinforced by a number of «opaque» coefficients, tabular and graphical dependencies. As a result, not only is the physical and mathematical meaning of DLR lost, but even the accuracy of its calculation is difficult to assess.

The problem of classical calculations of inductive leakage reactances is that their methods are based on simpler magnetic field models, oriented on the theory of magnetic circuits, which does not give sufficiently adequate results due to the complex geometry of the

electromagnetic system of TIMs and, accordingly, the structure of real magnetic fields.

In this sense, it is currently relevant to revise the conservative classical system of TIM design based on direct calculations of magnetic fields by numerical methods, for which there are appropriate software tools, for example, COMSOL Multiphysics, ANSYS Maxwell, FEMM, etc., which allow to avoid forced conventions and simplifications when determining the leakage reactances of TIM windings.

The use of various software complexes, as well as other experimental and computational studies of the characteristics and parameters of TIMs is reflected in a significant number of works, for example, in [3–21]. But, focusing on the implementation of a specific goal, each of them does not actually concern the analysis of the leakage reactances of TIM windings. This means that such works only use the data obtained during the classical design or creation of TIMs, but the analysis of these parameters does not occur. Therefore, the task of a detailed analysis of the methodology for calculating the leakage reactances of TIM windings remains insufficiently studied and is currently relevant.

This is especially true for the parameters of differential scattering of TIM windings, which are the least studied due to the complexity of the physical process of their formation, although the share of this scattering among its other components is usually predominant.

The goal of the work is to further develop the TIM design system through numerical-field calculation analysis of the differential leakage reactance of their stator winding, as well as a comparative check of the corresponding empirical formulas inherent in the methods of traditional design calculations.

Analysis of recent research. Despite the very long development and use of TIMs, research on their further study and improvement as such, as well as improving their operation in electric drive systems, continues on a fairly broad scale, for example, in works [3–10]. And these works to one degree or another affect the parameters of these motors.

Thus, in [3] for energy saving, an online estimation of TIM parameters using an extended Kalman filter is proposed. It is noted that to calculate the optimal value of the stator current for energy saving, its exact parameters are required, which are estimated in real time using an online estimator, and that this can ensure minimal power losses for the TIM drive.

The goal of the work [4] is to study the effectiveness of implementing fuzzy logic on FPGA programmable logic circuits for diagnosing failures of induction machines in case of phase asymmetry and their breaks. This is done on the basis of fuzzy logic and analysis of the motor stator current signals, its root-mean-square value.

In the article [5], a new method for diagnosing broken rotor bars in a lightly loaded induction machine in a stationary operation mode is provided. This method is used to solve the problem of using traditional methods, such as the Fourier transform signal processing algorithm, by analyzing the stator current envelope curve using discrete and continuous wavelet transform.

In [6], the development of a neural network model is presented, which allows generating a large database that can cover the maximum possible faults of the TIM stator. They take into account short circuits with large fluctuations in the machine load. The aim is also to automate the diagnostic algorithm using an artificial neural network classifier.

In [7], a comparative study of methods for taking into account the influence of loss processes in the stator steel of an asynchronous machine on the parameters of its operating mode was performed. This is done using mathematical modeling with the introduction of equivalent resistances connected in parallel to the equivalent circuit of the motor, as well as equivalent steel loss circuits.

The article [8] is devoted to the optimization of the design of an induction motor using multiparameter FEM methods. It is shown that the TIM parameters, including the types of rotor and stator slots, steel core sheets and rotor winding material, are optimized using the Rmxprt module in Maxwell.

In [9], the stages, methodology and means of complex design of electromechanical systems with induction motors are substantiated. A quantitative assessment of the possibilities of increasing their economic efficiency using complex design according to the criterion of maximum income is provided.

In [10], a flux linkage observer of an induction motor is considered, adaptive to variations in the active rotor resistance. Due to the redundant estimation of flux linkages introduced into the observer, under the conditions of persistence of excitation, the properties of global exponential stability of the estimation of the components of the flux linkage vectors and stator current and active rotor resistance are ensured.

The following cycle of works [11–21] mainly concerns the analysis of the active and reactive parameters of the stator winding, the use and improvement of TIM equivalent circuits, and operation with them.

In the work [11], the reactive (inductive) reactances of the scattering and active resistances of the TIM windings are investigated with the aim of further developing the TIM design system by means of numerical field calculation analysis of the active and reactive reactances of the TIM windings in the entire range of its slip change, and the calculation of the mechanical characteristics of the TIM to confirm the adequacy of the calculations of these resistances. The reactances of the TIM windings are determined by numerical calculations of the magnetic fields of scattering using the FEMM code, and in the core of the short-circuited rotor - with current displacement.

In the article [12], the magnetic fields and the corresponding magnetic conductivities of the slot scattering of the TIM stator winding are investigated for a comparative check of the analytical formulas from different classical design methods. The numerical field method shows that the classical design method can give both sufficiently accurate results and unacceptable errors in determining the magnetic conductivities of the slot scattering of the TIM.

In [13], it is emphasized that a deep understanding of the parameters of an induction machine is necessary for almost all program control methods to maintain high-quality dynamic and steady-state characteristics of the drive. This study presents a method for predicting the parameters of an induction machine during start-up without using any assumptions. The instantaneous waveforms of voltage and current recorded during direct start-up are used to estimate the parameters. In this way, all six main electrical parameters of induction machines can be independently determined.

In [14], a new simplified method for estimating the parameters of the equivalent T-circuit of induction motors is described, which is based solely on the manufacturer's data sheet and on the synergistic interaction of the numerical and analytical dimensionless approach using the Thevenin theorem. This provides accurate and stable results for a wide range of rotational speeds and power of induction motors.

In [15], the work is also devoted to estimating the parameters of the equivalent T-circuit. These parameters are necessary for many performance and planning studies involving these motors. For their evaluation, an iterative method is proposed that uses only motor nameplate data.

In [16] it is emphasized that for controlling the torque in high-performance operations in a wide speed range by vector control algorithms, the parameters of the equivalent circuit of an induction motor must be known precisely. The estimation method is based on information from the manufacturer's data and the principles of solving nonlinear equations obtained from the equivalent circuit of such a motor.

The article [17] is devoted to the identification of the parameters of an induction motor in a stopped state. A comprehensive identification procedure is analyzed, which describes a method for reliably determining the characteristics of the main flux saturation and transients when testing the parameters from the rotor side. The effect of the main flux saturation is studied based on the results of transient tests and the determined rotor parameters. The identification procedure is confirmed by experiments using specific induction motors.

How to design a TIM with the desired characteristics and how to implement high-performance control for a specific TIM has always been a hot topic for many researchers, as noted in [18]. Regardless of which control technology is used to achieve high-performance TIM drive, it depends on a deep understanding of the motor parametric characteristics and their accurate acquisition. An effective method for determining the parameters of the equivalent circuit for induction motors is proposed to improve the accuracy of the parameters by combining the non-rotor test with the double-load test and using this method to measure and analyze the parametric characteristics of TIM.

In [19], a study of the degree of unbalance and the differential magnetic leakage coefficient of electrical machines equipped with multiphase windings is presented. The analysis was carried out for 4800 combinations between slots/poles/phases/layers, considering the changes in the leakage factor for each condition and determining the optimal zone for minimizing the leakage. The results show that the leakage coefficient can be significantly reduced by using slightly asymmetrical windings.

In the article [20], an accurate and simple method for determining differential dissipation factors in multiphase AC electric machines with asymmetrical windings is provided. The method is based on the properties of Görges polygons, which are used to transform an infinite series expressing the differential dissipation factor into a finite sum in order to significantly simplify the calculations.

The work [21] introduces the estimation of TIM parameters based on a differential evolution algorithm aimed at estimating its electrical and mechanical parameters. A comparative study of the results using three different input signals is carried out. Such an algorithm is able to estimate the parameters of the equivalent electrical circuit, such as stator and rotor resistances and leakage inductances, magnetizing inductance, as well as mechanical parameters, such as the moment of inertia and the friction coefficient.

Object of study. To generalize the research of DLR, they are performed for a number of TIM variants, which have in common the nominal phase voltage U_{sN} = 220 V and frequency f_s = 50 Hz; accordingly, the number of phases m_s = 3.

The basic one is a four-pole TIM with nominal power P_N = 7.5 kW, which is interesting in that it is a test object in the design methodology [1], which is still widespread at enterprises and Universities of the corresponding profile.

A total of nine similarly designed TIM variants with variable power of 4; 7.5 and 11 kW are considered, each of which is considered with the number of pole pairs p equal to 1, 2 and 3.

Motors with such parameters are quite common in modern production of TIM of general industrial execution [22, 23]. Thus, the nine adopted variants will allow us to sufficiently fully demonstrate the results of calculations using the numerical field method adopted here and compare them with the results using the classical method.

The main design parameters of the selected TIM variants are given in Table 1. They were obtained using the classical method [1], which was converted into an author's Lua script included in a single software package based on the FEMM code [24]. This script was tested on the specified basic TIM variant, which eliminates design errors of various origins.

Table 1

The most important design data of TIN

P_N	p	h	d_s	l_s	δ	q_s	Q_s	N_s	Q_r	I_{sN}
kW	–	mm	mm	mm	mm	–	–	–	–	A
4	1	100	96	110	0,45	4	24	132	19	7,92
	2	100	109	145	0,30	3	36	144	28	8,74
	3	112	134	140	0,30	3	54	171	51	9,29
7,5	1	112	109	140	0,50	4	24	88	19	15,42
	2	132	147	120	0,35	3	36	126	34	15,31
	3	132	158	155	0,35	3	54	135	51	15,94
11	1	132	129	135	0,60	4	24	76	19	22,23
	2	132	147	165	0,35	3	36	90	34	22,26
	3	160	192	135	0,40	3	54	126	51	22,85

Table 1 indicates the TIM parameters: h – height of the rotation axis, d_s, l_s – inner diameter of the stator core bore and its axial length; δ – air gap; q_s – number of slots per pole and stator phase; N_s – number of consecutive turns in the phase winding; Q_s, Q_r – number of stator and rotor slots; I_{sN} – nominal stator phase current.

The general layout of the TIM is given in Fig. 1.

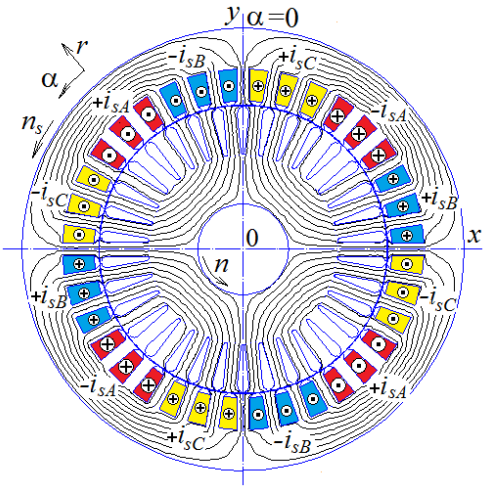

Fig. 1. The electromagnetic system of the TIM with the distribution of currents in its windings and the pattern of the magnetic field lines of the stator winding

The stator winding is single-layer, diametrical, which is typical for TIMs of the specified powers, the rotor winding is short-circuited, cast from aluminum alloy. This TIM uses common shapes of stator and rotor slots of general industrial TIMs [1, 2, 22, 23], which are shown in Fig. 1.

Design methodology for determining the differential inductive reactance of the stator winding of the TIM. For the transparency of the research performed, the classical methodology for calculating the DLR according to [1] and the results obtained by it are first given.

Differential scattering magnetic conductivity coefficient

$$\lambda_{sd} = 0{,}9\frac{(\tau_s \cdot K_{Ws})^2 \cdot K_{r\,dm} \cdot K_{ns} \cdot K_{dif\,s}}{\delta \cdot K_C}, \qquad (1)$$

where $K_{ns} = 1 - \frac{0{,}033 \cdot b_{s1}^2}{\tau_s \cdot \delta}$ is the coefficient that takes into account the effect of opening the stator slots; b_{s1} is the slot width of its slots; τ_s is the stator tooth pitch; $K_{dif\,s}$ is the stator differential dissipation coefficient, equal to the ratio of the total EMF from the higher harmonics of the stator magnetic field to the EMF from the first harmonic, determined by Table 2; $K_{r\,dm}$ is the damping reaction coefficient of currents induced in the short-circuited rotor winding by the higher harmonics of the stator magnetic field, determined by Table 3 for the given TIM variants; K_{Ws} is the stator winding coefficient; K_c is the air gap coefficient.

Table 2

Determination of the stator differential dissipation coefficient

q_s	2	3	4	5	6
$K_{dif\,s}$	0,0285	0,0141	0,0089	0,0065	0,0052

Table 3

Determination of the damping reaction coefficient of rotor winding currents (fragment of the general table)

q_s	Values $K_{r\,dm}$ at Q_r / p				
	10	15	20	25	30
3	0,98 / 0,92	0,93 / 0,87	0,88 / 0,84	0,85 / 0,78	–
4	–	0,90 / 0,81	0,84 / 0,77	0,8 / 0,75	0,77 / 0,72
Value: in the numerator – with bevel of the rotor slots, in the denominator– with no bevel.					

Data for (1) for all TIM variants according to Table 1 are collected in Table 4.

The intrinsic conductivity coefficient of differential scattering λ_{sd} of the stator winding together with other similar values are given in Table 5, where it is indicated: λ_{sn}, λ_{sfh} – magnetic conductivity coefficients of slot and frontal scattering; $\lambda_{\sigma s}$ – total scattering coefficient; R_s, $X_{\sigma s}$ – total active and reactive resistances of the stator winding in the nominal operating mode of the TIM, and also X_{sd} – reactive resistance of differential scattering.

Table 4

Data for design calculation of the coefficient of magnetic conductivity of differential scattering of TIM

P_N	p	τ_s	b_{s1}	K_c	K_{Ws}	$K_{r\,dm}$	$K_{n\,s}$	K_{dif}
kW	–	mm	mm	–	–	–	–	–
4	1	12,6	3,0	1,204	0,958	0,852	0,95	0,0089
	2	9,5	3,0	1,349	0,960	0,940	0,90	0,0141
	3	7,8	3,2	1,521	0,960	0,910	0,86	0,0141
7,5	1	14,3	3,2	1,179	0,958	0,852	0,95	0,0089
	2	12,8	3,5	1,283	0,960	0,910	0,91	0,0141
	3	9,2	3,5	1,433	0,960	0,910	0,88	0,0141
11	1	16,9	3,5	1,150	0,958	0,852	0,96	0,0089
	2	12,8	3,5	1,283	0,960	0,910	0,91	0,0141
	3	11,2	3,8	1,360	0,960	0,910	0,89	0,0141

Table 5

Calculated design resistances of TIM

P_N	p	λ_{sn}	λ_{sd}	λ_{sfh}	$\lambda_{\sigma s}$	R_s	X_{sd}	$X_{\sigma s}$
kW	–	p.u.	p.u.	p.u.	p.u.	Ω	Ω	Ω
4	1	1,261	1,729	1,805	4,794	1,771	0,654	1,815
	2	1,377	2,200	0,704	4,281	1,842	0,871	1,695
	3	1,521	1,215	0,676	3,413	2,103	0,437	1,226
7,5	1	1,257	2,060	1,575	4,892	0,744	0,441	1,047
	2	1,365	3,55	1,089	6,014	0,834	0,893	1,508
	3	1,532	1,573	0,704	3,809	0,941	0,390	0,945
11	1	1,254	2,487	1,884	5,625	0,452	0,383	0,866
	2	1,355	3,559	0,789	5,704	0,487	0,626	1,004
	3	1,653	2,180	0,958	4,791	0,673	0,410	0,901

Note that the relative value of the differential scattering conductivity coefficient λ_{sd} in $\lambda_{\sigma s}$ is a fraction within 0.361–0.624, which shows a high specific weight of this type of scattering against the background of its other types.

The inductive resistance of the scattering of the phase winding of the stator is calculated by the well-known formula [1]:

$$X_{\sigma s} = 1{,}58 \cdot \frac{f_s \cdot l_s \cdot N_s^2 \cdot \lambda_{\sigma s}}{p \cdot q_s \cdot 10^8}, \qquad (2)$$

and the differential leakage reactance X_{sd} – according to a similar formula when replacing $\lambda_{\sigma s}$ with λ_{sd}.

The provision in Table 5 of the active resistance R_s of the stator winding along with its total reactive reactance $X_{\sigma s}$ indicates their proportionality and importance of both in calculating important operational parameters and characteristics of TIMs and their operating modes [1, 2].

Numerical field calculations of the parameters of differential scattering of the stator winding of the TIM. The physically transparent path to the DLR lies through the direct calculation of the harmonic composition of the EMF of the stator winding, which are determined directly through the time functions of its own magnetic flux linkage (MFL) [25]. All this can be done in the most reliable form on the basis of numerical calculations of the corresponding magnetic fields of the stator winding itself.

These magnetic fields in the TIM are calculated in the popular free software package FEMM [24]. Given the multivariate complex calculations that include the design of the TIM, the construction of its physical and geometric models in the FEMM software environment, control of magnetic field calculations, determination of the time functions of the MFL and EMF and their harmonic analysis, all of them were automated. For this, following the example in [26] and other works of the author, a single script was created in the algorithmic language Lua, integrated into the FEMM code.

The FEMM code solves a large system of algebraic equations, which are formed on the basis of the Finite Element Method and a differential equation describing the magnetic field in the cross section of the TIM electromagnetic system, namely [24]:

$$\nabla\times\left[\frac{1}{\mu(B)}\nabla\times(\vec{k}A_z)\right]=\vec{k}J_z\,, \qquad (3)$$

where J_z, A_z are the axial components of the current density vectors and the magnetic vector potential (MVP); μ is the magnetic permeability depending on the magnetic flux density B; $\vec{k}$ is the unit vector along the axial axis z.

To limit the TIM calculation zone, which is given in Fig. 1, the Dirichlet boundary condition is set on the outer surface of the stator core for the MVP, i.e. $A_z = 0$.

A feature of this study is that to determine the differential inductive resistance of the stator winding, the basis is the calculation of the magnetic field of this winding in the presence of a symmetrical three-phase system of phase currents in it

$$\begin{aligned} i_{sA} &= I_{ms}\cos(\omega t)\,; \\ i_{sB} &= I_{ms}\cos(\omega t-\tfrac{2}{3}\pi)\,; \\ i_{sC} &= I_{ms}\cos(\omega t+\tfrac{2}{3}\pi)\,, \end{aligned} \qquad (4)$$

where $I_{ms}=\sqrt{2}\cdot I_s$ is the amplitude of the currents; I_s, $\omega = 2\pi f_s$ are their effective value and angular frequency; t is time.

When forming the current system (4) in specific calculations of magnetic fields, the question arises of choosing the calculated effective value of the current I_s.

The guideline for the calculations is that the saturation of the magnetic system of the TIM should be at the same level as in its nominal operating mode. Accordingly, for the stator winding, the value of the current of the idealized idle mode (IIM) is taken as a first approximation, which provides this condition. Naturally, there are no currents in the rotor winding in this mode.

The model in Fig. 1 shows the accepted distribution of the phase zones of the stator winding, and the values of the phase currents in them are given by (4) for specific moments of time. So at $t = 0$ we have the corresponding instantaneous values of the currents: is $i_{sA}=I_{ms}$; $i_{sB}=i_{sC}= -0.5I_{ms}$, and their directions at the specified time are also indicated.

The conditional distribution of currents in the slots of the stator winding is shown in Fig. 2 as a discrete function in the angular coordinate α, which is indicated in Fig. 1, and in the pole steps τ_p. The points that reflect the currents in the slots are meaningful, and the connecting lines are drawn for clarity of the current structure.

For the FEMM code, the numerical solution of equation (1) by the Finite Element Method is a trivial problem. As a result, in the cross section of the TIM, the distribution of the MVP is obtained, which in Fig. 1 gives a picture of the magnetic field lines in the idealized idle mode. Here and further, current illustrations are provided on the example of the adopted basic TIM model.

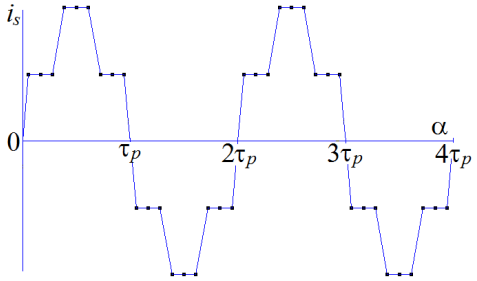

Fig. 2. Angular discrete distribution of currents is of the stator winding of the TIM along its slots on the scan of the cylindrical surface in the gap

The next step of the calculations is to determine the magnetic flux linkage (MFL) of the stator phase winding, as which, as usual, the phase winding A with current i_{sA} is taken. For the MFL in the FEMM code and the Lua script there are corresponding procedures. But what is needed is not just one value of the MFL, but its angular, and then the time function.

For this, there are two ways of calculations: fast and long-term, which we will consider in turn.

A fast method for forming time functions of the MFL and EMF is appropriate at the initial stage of numerical field studies of the DLR.

In this case, the angular function of the MFL is first obtained after a one-time calculation of the magnetic field at $t = 0$, the picture of which is already shown in Fig. 1 and corresponds to a fixed distribution of the MVP.

Specifically, according to the distribution of the MVP in the cross section of the TIM, the values of the MFL of the phase winding A are «collected» with the alternate selection of the «mask» of the phase zone with its movement in the angular direction along the slot structure of the stator.

Figure 3 shows the sequence of such actions for moving the «mask» within two pole steps, which corresponds to the period of the angular function of the MFL.

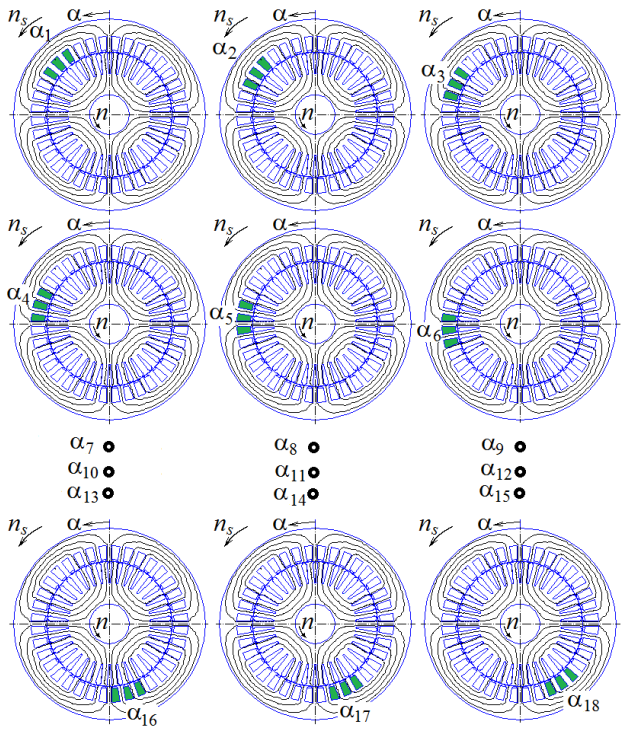

Fig. 3. The process of moving the «mask» of the phase zone of the stator winding to collect the MFL within the period of its angular function against the background of the calculated magnetic field

In each selected position, the Lua commands Ak=mo_blockintegral(1) and Sk=mo_blockintegral(5) read the surface integral of the MVP and the area of the selected block of rods, which makes it possible to determine the MFL of the conditional phase zone with number k:

$$\Psi_k = N_s A_k / S_k. \quad (5)$$

Thus, a discrete angular function of the MFL appears

$$\Psi_k(\alpha_k); \quad \alpha_k = (k-1)\tau_s; \quad k = 1, 2, 3, \ldots K, \quad (6)$$

where k is the counter of the positions of the conditionally movable «mask» of the phase zone; $K=Q_s/p$ is the number of such positions within two pole steps τ_p, which is the period T of the function (6); $\tau_s=360°/Q_s$ is the stator tooth step.

The resulting numerical array of the MFL is given in Table 6.

Table 6

Angular discrete function of the MFL Ψ_k of phase zones of phase winding A in 18 angular positions, Wb

k	1	2	3	4	5	6
Ψ_k	0,4858	0,4555	0,3708	0,2418	0,0840	–0,0840
k	7	8	9	10	11	12
Ψ_k	–0,2418	–0,3707	–0,4554	–0,4858	–0,4512	–0,3644
k	13	14	15	16	17	18
Ψ_k	–0,2366	–0,0819	0,0819	0,2366	0,3644	0,4512

The angular function at two pole steps, i.e. at its period (Table 6), is in principle sufficient to give an idea of its essence, but for the first attempt similar actions were performed at two more pole steps and the result was completely repeated. The resulting discrete function Ψ is shown in Fig. 4.

The angular discrete function of the $\Psi_k(\alpha_k)$ of the phase zones according to Table 6 is transformed into a similar function for the phase winding A entirely at its period:

$$\Psi_{s,k} = \Psi_k(\alpha_k) - \Psi_{k+K/2}(\alpha_k + \tau_p); \; k = 1, 2, 3, \ldots K. \quad (7)$$

Here it is taken into account that the winding branches are formed by conductors in phase zones with different current directions, located through the pole step τp. In addition, the averaging of the MFL values of the phase zones located through two pole steps is obtained, due to which instead of the function Ψ in Fig. 4 over two periods, the averaged MFL function Ψ_s over one period within two pole steps is obtained. This function is illustrated in the same Fig. 4.

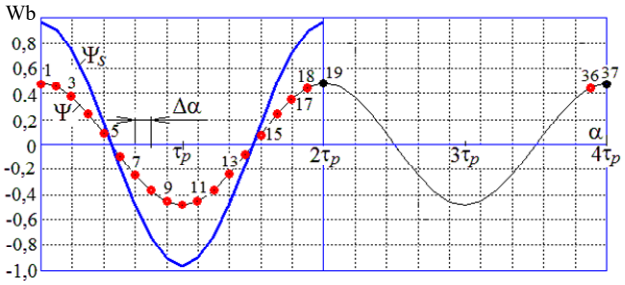

Fig. 4. Angular function of the MFL phase zones of half of the phase winding – Ψ and the phase winding in full – Ψ_s

It turned out that the angular function of the MFL is close to the cosine, as well as the time functions of the phase currents (4), but it is fundamentally different from the angular function of the current distribution in the slots (Fig. 2). However, in the theory of TIM, based on the step function of the stator currents is(α), it is customary to form similar functions of the distribution of the magnetomotive force (MMF) in the gap, then – of the magnetic induction and magnetic fluxes. And all this is laid down as the basis for the harmonic analysis of magnetic and electrical quantities, including – the EMF in the phase windings of the stator.

But the inadequacy of this approach is shown in [27] on the example of a three-phase stator winding of a turbogenerator. This is confirmed by the practically harmonic function of the MFL (Fig. 4), from which there is only one step left to a similar, but time, EMF function.

The function Ψ_s (7) is periodic, therefore it is subject to expansion into a harmonic Fourier series on its period in two pole steps (see Fig. 4), on which the MFL is calculated at K points (their specific number in this TIM is 18, and point 19 is already included in the next period and repeats point 1).

The expansion begins with the determination of the sine and cosine amplitudes of the harmonic components:

$$s_\nu = \frac{2}{K}\sum_{k=1}^{K}\Psi_k \sin(\nu\alpha_k); \quad c_\nu = \frac{2}{K}\sum_{k=1}^{K}\Psi_k \cos(\nu\alpha_k), \quad (8)$$

where ν is the number of the current harmonic; k is the number of the angular position in Fig. 3, 4; α_k is its angular coordinate.

It is known from mathematical foundations that the maximum number of harmonics allowed is $N_g = K/2$.

Considering that cosine functions (4) are adopted for the stator winding currents, then for the MFL, the harmonic series of cosine functions is also determined by the coefficients (8):

$$\Psi = \sum_{v=1,3,5...}^{N_g} \Psi_{mv} \cos(v\alpha + \gamma_{\psi v}), \qquad (9)$$

where this series for each harmonic includes the following amplitude and argument (initial phase):

$$\Psi_{mv} = \sqrt{s_v^2 + c_v^2}\ ; \quad \gamma_{\psi v} = -\text{arctg}\frac{s_v}{c_v}. \qquad (10)$$

The angular function (9) is converted into a time function by the relation $\alpha=\Omega_s t$, where $\Omega_s=\omega/p$ is the angular velocity of the rotating magnetic field of the TIM. As a result, for the MFL, a harmonic time function is obtained, which corresponds to the stationary phase winding *A–A*:

$$\Psi = \sum_{v=1,3,5...}^{N_g} \Psi_{mv} \cos(v\omega t + \gamma_{\psi v}). \qquad (11)$$

Note that in (9) the quantities $v\alpha$ and $\gamma_{\psi v}$ are measured in angular radians or degrees, and in (11) the quantities $v\omega t$ and $\gamma_{\psi v}$ are measured in electrical radians or degrees, taking into account the known transition of geometric angles α into electrical α_{el}, i.e. $\alpha_{el}=p\alpha$.

From the MFL function (11) based on the law of electromagnetic induction according to the general expression $e = -d\Psi/dt$, a transition is made to the harmonic time function of the EMF of the stator phase winding:

$$e_s = \sum_{v=1,3,5...}^{N_g} v\omega\Psi_{mv} \cos\left(v\omega t + \gamma_{\psi v} - \pi/2\right). \qquad (12)$$

In this formula, the amplitude of the EMF of the *v*-th harmonic is extracted

$$E_{mv}=v\omega\,\Psi_{mv} \qquad (13)$$

and its corresponding initial phase

$$\gamma_{ev} = \gamma_{\psi v} - \pi/2. \qquad (14)$$

Also, according to the known relationship for a sinusoidal function, the effective value of the EMF of the *v*-th harmonic is obtained through the amplitude, namely:

$$E_{sv} = \sqrt{2}\pi f_s v\Psi_{mv}, \qquad (15)$$

where it is taken into account that the angular frequency $\omega=2\pi f_s$; f_s is the frequency of electromagnetic quantities in the TIM.

The angular functions (6), (7) in Table 6 and Fig. 4, respectively, have a semi-periodic asymmetry:

$$\Psi_{s,k}(\alpha_k) = -\Psi_{s,k}(\alpha_k + \tau_p);\ k = 1, 2, 3, ...K, \qquad (16)$$

therefore, the harmonic series (9), (11), (12) contain only odd harmonics.

According to the provided method in the form of formulas (5)–(15), a corresponding software implementation of the formation and expansion of the periodic MFL function into a harmonic Fourier series and obtaining a similar EMF function was made on the Lua script.

Determination of the magnetizing current of the stator winding. As noted, the magnetic field calculations are performed in the IIM under the condition of saturation of the magnetic core equivalent to the nominal mode. For this, the search for the corresponding current is introduced into the calculation structure after the design of the TIM. This occurs iteratively provided that the nominal voltage of the stator winding U_{sN} is reached.

The initial current value for the first iteration is the design value of the magnetizing component of the stator winding current I_{so}, which is equal to 5.65 A.

After calculating the magnetic field, the time function of the MFL (11) and then the EMF (12) are determined using the above method, for which the first harmonic is isolated and used, namely, for the EMF – its effective value E_{s1} (15) and the initial phase γ_{e1} (14).

This is enough to determine the phase voltage complex in symbolic form according to the voltage balance equation in the stator phase winding circuit.

$$\underline{U}_s = -\underline{E}_{s1} + \underline{U}_{Rs} + \underline{U}_{s\sigma dif} + \underline{U}_{s\sigma fh}, \qquad (17)$$

where the complexes are applied: EMF $\underline{E}_{s1} = E_1 e^{j\gamma_{e1}}$; voltage drop across the active resistance of the stator winding $\underline{U}_{Rs} = R_s\underline{I}_{so}$ and on the inductive resistances of its differential $\underline{U}_{s\sigma dif} = jX_{sd}\underline{I}_{so}$ and frontal $\underline{U}_{s\sigma fh} = jX_{sfh}\underline{I}_{so}$ scattering (the inductive resistance of the slot scattering is already taken into account in the EMF $\underline{E}_{s1}$ due to the definition of the full MFL of the stator winding (5) within its active part along the length of the TIM cores); the stator winding current complex has the form $\underline{I}_{so}=I_{so}$ due to the fact that a zero initial phase is assumed for it.

After determining the voltage at the current iteration, the magnetizing current at the next iteration is corrected by linear interpolation, and everything is repeated until the voltage deviation dU_s from its nominal value is reduced to the permissible level. The course of the iterative process is illustrated in Table 7, where n_i is the iteration number.

Table 7

Changes in magnetizing current in the iterative process of bringing the voltage to the nominal value

n_i	I_{so}, A	U_s, V	dU_s, V
0	5,65	240,9	20,86
1	5,16	224	4,01
2	5,05	221,2	1,25
3	4,99	219,9	–0,06
4	4,99	220	0

In this example, it is clear that at the design value of the magnetizing current, the voltage deviates quite significantly from the nominal, which is a consequence of the use of magnetic calculation based on the theory of magnetic circuits in the design. But the iterative process showed that to operate with the nominal voltage, and therefore with the corresponding saturation of the TIM magnetic core, the magnetizing current should be 4.99 A. This is the value of I_{so} that is used for further calculations of the test TIM in the IIM and determining its DLR.

As a result of further calculations and harmonic analysis of the angular functions of the MFL and EMF on the period, the following calculated data are obtained: amplitude and initial phase of the first harmonic of the MFL Ψ_{m1}= 0.9640 Wb; $\gamma_{\psi 1}$=0; effective value and initial

phase of the same harmonic of the EMF E_{s1}= 214.1 V; γ_{e1}= –90°.

The harmonic composition of these quantities in relative units (p.u. is given in Table 8 (the value of their first harmonics is taken as the basis), and the allowed number of harmonics N_g was 9.

Table 8

Harmonics composition of MFL and EMF

ν	–	1	3	5	7	9
$\Psi_{m\nu}$	p.u.	1,000	0,0047	0,0017	0,0010	0,0009
$E_{m\nu}$	p.u.	1,000	0,0141	0,0087	0,0070	0,0078
$E_{s\nu}$	V	214,1	3,02	1,87	1,51	1,68

In general, the harmonic composition is estimated by the distortion factor (using the example of EMF)

$$d_{distE} = \sqrt{\sum_{\nu=1}^{N_g} E_{m\nu}^2} \Big/ E_{m1}\,, \qquad (18)$$

which for the functions of MFL and EMF received the corresponding values: $d_{distΨ}$= 1.0000; d_{distE}=1.0002.

Taking into account the entire determined harmonic composition, the equivalent effective value of the phase EMF of the stator winding is found

$$E_s = \sqrt{\sum_{\nu=1,3,5...}^{N_g} E_{s\nu}^2}\,, \qquad (19)$$

as well as differential EMF, which consists only of higher harmonics,

$$E_{sdif} = \sqrt{\sum_{\nu=3,5...}^{N_g} E_{s\nu}^2}\,. \qquad (20)$$

The last EMF allows to determine the desired differential inductive resistance of the stator phase winding:

$$X_{sdif} = \frac{E_{sdif}}{I_{so}}. \qquad (21)$$

Calculations using (19)–(21) gave the following results: E_s= 214.2 V; E_{sdif} = 4.21 V; X_{sdif} = 0.84 Ω.

If we compare the obtained differential inductive resistance X_{sdif} = 0.84 Ω with its design value X_{sd} = 0.893 from Table 5, we can think about the closeness of the two calculation options.

But this is until similar calculations have been performed for all planned TIM options (Table 1): all the results obtained are given in Table 9, where for different options, according to their data, the number of available harmonics N_g was 9 or 11.

Table 9

Differential parameters of TIM obtained by a single numerical-field calculation of the magnetic field

P_N	p	I_{so}	Ψ_{m1}	E_{s1}	E_s	E_{sdif}	X_{sdif}
kW	–	A	Wb	V	V	V	Ω
4	1	2,56	0,9747	216,5	216,5	1,99	0,78
	2	3,84	0,9700	215,5	215,7	10,16	2,65
	3	6,34	0,9691	215,3	215,8	14,54	2,29
7,5	1	4,39	0,9749	216,6	216,6	1,99	0,45
	2	4,99	0,9640	214,1	214,2	4,21	0,84
	3	7,99	0,9694	215,3	215,6	10,01	1,25
11	1	5,95	0,9723	216,0	216,0	2,05	0,34
	2	7,17	0,9655	214,5	214,5	4,25	0,59
	3	9,06	0,9658	214,6	214,6	6,33	0,70

In relation to the data in Table 9, we note that the distortion coefficients are within the limits: $d_{distΨ}$=1.0000–1.0002; d_{distE}=1.0000–1.0023, i.e. the corresponding angular functions of the MFL and EMF, as in Fig. 4, are close to their first harmonics. This is also evidenced by the closeness of the values of E_{s1} and E_s.

As for the main quantity considered here, i.e. the differential leakage reactance, its values X_{sd} та X_{sdif}, obtained by different methods in Table 5 and 9, can be both close and significantly diverge.

This indicates the absence of strict determinism of the empirical formula (1) and a number of coefficients included in it.

At the same time, the numerical-field method does not have such drawbacks, because it has fewer weighty conventions and assumptions. But in the considered form, it also has a serious drawback, namely – a small number of harmonics, which is associated with a limited number of calculation positions (see Fig. 3) due to the available number of stator slots at two pole steps, that is, at the period of the MFL and EMF functions.

To solve the identified problem, it is necessary to involve a more accurate calculation method. And as such, the numerical-field method is again adopted, but one that allows you to involve the desired number of calculation positions and, accordingly, the number of harmonics in the calculations.

The long-term method of forming the time functions of the MFL and EMF is appropriate at the final stage of numerical field studies of the DLR.

In this case, the time function of the MFL of the stator winding is considered directly without its previous angular function.

To obtain the time function of the MFL, multi-position calculations of the magnetic field are performed alternately, as shown in [25, 27], for a time series with a step Δt:

$$t_k = \Delta t\,(k–1); \quad k = 1,2,...,K, \qquad (22)$$

where K is the number of positions that allows forming a time function at a given time interval.

Substituting these values of t_k into (4), we obtain the corresponding changes in the stator phase currents is and their wave, which moves in angular $\Delta\alpha=\Omega_s\cdot\Delta t$, where $\Omega_s=2\pi f_s/p$ is the already mentioned angular velocity of the rotating magnetic field.

The calculation of the stator currents (4) at given moments of time (22), as well as the calculation and collection of the MFL values (5) were performed automatically during the operation of the FEMM code using the already mentioned program in the Lua language.

In this case, the magnetic field rotates, and the phase zones for collecting MFL values are stationary, which is partially shown in Fig. 5.

As before, the phase zones were selected for phase winding A (see Fig. 1), but in the order that explains Fig. 6.

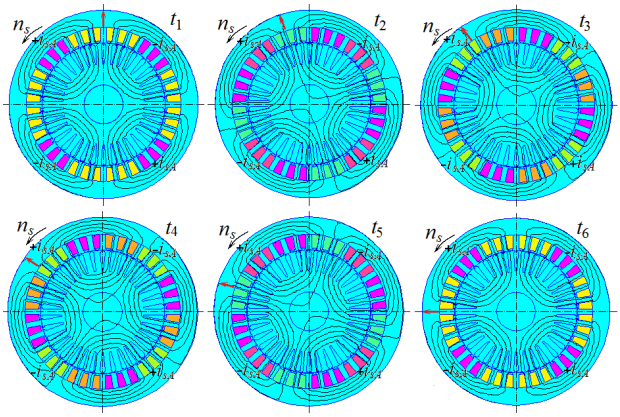

Fig. 5. Pictures of the rotating magnetic field of the stator winding at fixed moments of time:
t_1=0; t_2=0.1T; t_3=0.2T; t_4=0.3T; t_5=0.4T; t_6=0.5T

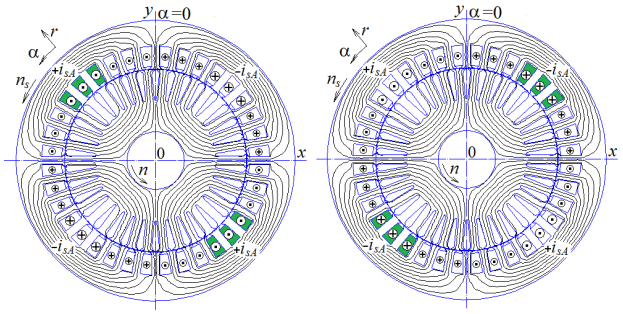

Fig. 6. Selection of phase zones of the stator winding to obtain the MFL of the stator phase winding

First, phase zones with a conditional positive current direction $+i_{sA}$ are distinguished and their MFL Ψ_{is+} is obtained, then phase zones with a conditional negative current direction $-i_{sA}$ are distinguished and their MFL Ψ_{is-}. is obtained.

As a result, a time discrete function of the MFL of the phase winding of the TIM stator at specific moments of time with a change in their number k is obtained:

$$\Psi_{s,k} = \Psi_{is+,k} - \Psi_{is-,k}\ ;\ t_k;\ \ k = 1, 2, 3, ...K. \qquad (23)$$

Then everything happens as in the previous calculation method, that is, according to (10)–(15), starting with the harmonic expansion of the discrete time function (23) instead of the similar function (9).

It is determined that it is enough to step by step (22) pass one pole step of the TIM τ_p, which will correspond to half the period T of the time function of the MFL $\Psi(t)$ and the calculation zone (in degrees):

$$\alpha_z = 360° / 2p, \qquad (24)$$

and in the test four-pole TIM α_z = 90° specifically turns out.

To justify a sufficient number of calculated positions K, comparative calculations were performed at different values of K. Thus, it was determined that the value of K = 27 is sufficient, and then the angular step (in degrees):

$$\Delta\alpha = \alpha_z / K = 3.333°. \qquad (25)$$

This provides a satisfactory detailing of time functions of type (23). At the same time, the calculation time for one TIM on a sufficiently high-level computer lasted about 1 hour.

The obtained time function of the stator phase winding is shown in Fig. 7: in the first half of the period, this is what was obtained by calculation, in the second half, the full period is drawn for clarity under the condition of semi-periodic asymmetry of type (16). With the selected number of points, the graph of the MFL function looks quite smooth (unlike the similar function in Fig. 5), and the number of its harmonic components can be taken up to N_g = 27, which corresponds to the number of points in half the period.

To analyze the MFL function, it was decomposed into a harmonic series similar to (11), and then a transition was made to the EMF harmonic series (12). The values of the amplitudes of the EMF harmonics in p.u. and their corresponding effective values in absolute terms are given in Table 10, but only up to the 19th harmonic out of 27 possible, because the higher harmonics were then negligible.

Calculations using (19)–(21) gave the results: E_s= 215.4 V; E_{sdif} = 4.59 V; X_{sdif} = 0.92 Ω.

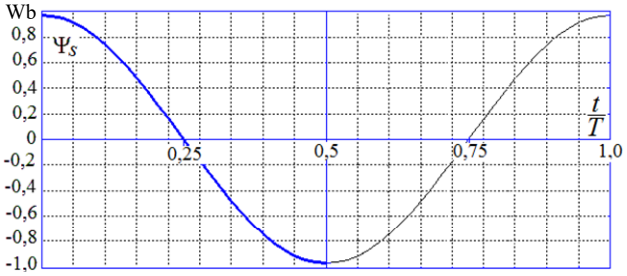

Fig. 7. Time function of the MFL of the phase winding of the TIM stator

Table 10

Harmonic composition of the stator winding EMF

ν	–	1	3	5	7	9
E_{mv}	p.u.	1,000	0,0144	0,0155	0,0020	0,0011
E_{sv}	V	215,3	3,10	3,33	0,43	0,25
ν	–	11	13	15	17	19
E_{mv}	p.u.	–	0,0012	0,0006	0,0000	0,0005
E_{sv}	V	0,04	0,26	0,14	0,09	0,11

These results are again quite close to those obtained by other calculation methods (X_{sdif} = 0.84 Ω, X_{sd} = 0.893 Ω), although they differ from them, with a discrepancy of X_{sdif} of 9.5 %.

But the same closeness of the results by comparative calculation methods is not maintained for other TIM variants, for which the results are summarized in Table 11.

Table 11

Differential parameters of different TIMs obtained by multiple numerical-field calculations of the rotating magnetic field

P_N	p	I_{so}	Ψ_{m1}	E_{s1}	E_s	E_{dif}	X_{sdifm}
kW	–	A	Wb	V	V	V	Ω
4	1	2,56	0,9818	218,1	218,2	5,51	2,15
	2	3,84	0,9815	218,0	218,2	7,93	2,07
	3	6,34	0,9696	215,4	215,9	14,67	2,31
7,5	1	4,39	0,9819	218,1	218,2	5,53	1,26
	2	4,99	0,9692	215,3	215,4	4,59	0,92
	3	7,99	0,9717	215,9	216,1	10,17	1,27
11	1	5,95	0,9791	217,5	217,6	5,28	0,89
	2	7,17	0,9712	215,7	215,8	4,71	0,66
	3	9,06	0,9703	215,5	215,6	6,46	0,71

Now we can compare the main calculation results for all TIM variants obtained by three different methods, which is done by the values of the differential inductive resistance of the TIM stator winding by collecting their values from Tables 5, 8, 11 to Table 12.

This table indicates: M1 – design data according to the standard method; M2 – data using a single numerical field calculation based on the angular functions of the MPZ; M3 – data using multi-position numerical field calculations based on the time functions of the MFL.

Table 12

Comparison of differential reactances of TIM obtained by different calculation methods

Calculation method			M1	M2	M3
P_N	p	I_{so}	X_{sd}	X_{sdif}	X_{sdif}
kW	–	A	Ω	Ω	Ω
4	1	2,56	0,654	0,78	2,15
	2	3,84	0,871	2,65	2,07
	3	6,34	0,437	2,29	2,31
7,5	1	4,39	0,441	0,45	1,26
	2	4,99	0,893	0,84	0,92
	3	7,99	0,390	1,25	1,27
11	1	5,95	0,383	0,34	0,89
	2	7,17	0,626	0,59	0,66
	3	9,06	0,410	0,70	0,71

Recall that for the M2 method, only 9 or 11 calculation points and the same number of harmonics was used, for the M3 method - 27 points, but it was even possible to limit ourselves to a smaller number.

The discrepancy between the values of X_{sd} and X_{sdif} by the M1 and M3 methods is impressive and excessively large in the majority of TIMs, which indicates the limitations of the classical method for calculating the differential reactance of the TIM stator winding. The same applies to the M2 calculation method in two-pole TIM variants.

The rather close correlation of the results of classical and numerical-field calculations for the basic TIM variant can be explained by the fact that in the methodology [1] the coefficients recommended for (1) were adapted specifically for this variant, but, unfortunately, they have not become universal for other TIM variants and still mislead their designers.

Upon completion of the studies of the differential parameters of the TIM when its magnetic system is saturated according to the nominal operating mode, calculated estimates of the effect of saturation on these parameters were made using the example of the basic TIM variant.

First of all, an example of a TIM with a completely unsaturated magnetic system was considered. For this, in the IIM, the current I_{so} was set to 1 A, and multi-position numerical field calculations were performed based on the time function of the MFL (23). The results of the calculations are given in the corresponding row of Table 13.

Table 13

Assessment of the effect of saturation of the TIM magnetic system on the differential reactance of the stator winding

I_{so}	$B_{r,ts}$	$B_{r,tr}$	$\mu_{r,ts}$	$\mu_{r,tr}$	E_s	E_{dif}	X_{sdifm}
A	T	T	p.u.	p.u.	V	V	Ω
1	0,44	0,38	2500	2490	48	0,04	0,04
5	1,84	1,61	787	1265	208	4,38	0,88
5,5	1,89	1,70	530	1010	224	7,05	1,28
6	1,96	1,78	414	835	238	10,1	1,68
10	2,21	2,06	132	265	302	36,7	3,67
15	2,30	2,20	64	238	339	59,7	3,98
50	2,36	2,28	29	77	369	83,5	3,34

To assess the saturation level of the magnetic system, the table provides the averaged values obtained for the sections of the magnetic core: $B_{r,ts}$, $B_{r,tr}$ – magnetic flux density in the stator and rotor teeth; $\mu_{r,ts}$, $\mu_{r,tr}$ – relative magnetic permeability in them (in the backs of the stator and rotor cores, the values of similar values were $\mu_{r,ys} = 5200$; $\mu_{r,yr} = 4920$).

The very weak saturation (or its absence) is also confirmed by the value of the phase EMF E_s, which turned out to be much lower than the nominal voltage of the TIM. As a result, the differential EMF E_{dif} and, accordingly, the DLR of the stator winding X_{sdifm} compared to the nominal saturation mode (see Table 12) almost did not appear.

The studies were continued at saturation levels of the magnetic core from the nominal to the one that can be at the start of the TIM. But in this case, it was necessary to take into account that with increased slips of the TIM from critical to 1, the stator and rotor currents simultaneously increase, and the voltage remains unchanged. Therefore, with increasing currents, the voltage drops on the active and reactive resistances of the windings increase, and the EMF has a reduced share. In proportion to the EMF, the main magnetic flux decreases and, accordingly, the value of the magnetic induction in the magnetic circuit.

The distribution of the magnetic field in the magnetic circuit in such a case and the level of its saturation require a careful analysis, which is difficult to conduct in detail within the framework of this article, and this can be performed and published separately.

In order to preliminarily assess how much such an analysis will give significant results and makes sense to perform, some conventions were adopted when calculating the magnetic field of the stator winding to determine the DLR.

Namely, that the saturation of the backs of the stator and rotor cores also maintains its level, as in the nominal mode. In fact, taking into account the remarks made, the saturation will be much lower, but this is not of principle, because even with a completely unsaturated magnetic core, the DLR does not differ very much from the results at nominal saturation. But the teeth of these cores saturate very strongly due to a significant increase in the magnetic fields of the slot and differential scattering, as explained in [2].

These assumptions provided the basis for organizing an artificial mode of calculating the DLR with strong saturation of the tooth portion of the TIM magnetic system.

Specifically, for the estimated calculations of the DLR with increased slips, the relative magnetic permeabilities in the backs of the stator and rotor cores were taken $\mu_{r,ys} = 1256$; $\mu_{r,yr} = 3666$ and they did not change when calculating the magnetic field. At the same time, the magnetic permeabilities in the core teeth were determined by the FEMM code as is customary in the process of such calculations.

The results of calculations of the specified variants of the TIM magnetic circuit are summarized in Table 13 at the specified values of the I_{so} current from 5 to 50 A. The data on the differential parameters at a value of 5 A

in principle correspond to the data in Table 11 at the standard operation of the FEMM code in the IIM of the TIM mode at current of 4.99 A.

The level of further saturation growth is reflected by the given averaged values of magnetic induction and relative magnetic permeability in the teeth of the stator and rotor cores. At the same time, the differential parameters of the TIM (EMF and DLR) increase significantly, which is associated with the redistribution of the magnetic field in the gap between the stator and rotor cores with an increase in the saturation of their teeth. And because of this, the higher harmonic components of the MFL and EMF of the stator winding increase significantly.

It can be seen from Table 13 that with an increase in current in the stator winding, the rate of DLR growth slows down compared to the increase in current, and even in the case of oversaturation of the teeth, this reactance reaches a maximum and even begins to decrease.

Conclusions.

1. In the system of design and theoretical research of TIMs, a significant place is given to the leakage reactances of their windings. They are determined on the basis of the theory of magnetic circuits, which in the conditions of complex tooth-and-groove structures does not guarantee the desired accuracy of calculations. This especially applies to the differential leakage reactance of the stator winding, the determination of which requires a detailed calculation of the magnetic field in the gap between the stator and rotor cores, and a harmonic analysis of the EMFs of this winding induced by it.

2. It is shown that in the current classical methods of designing DLR, they are determined by a simplified formula with the addition of a number of coefficients, tabular and graphical dependencies. As a result, not only is the physical and mathematical meaning of DLR lost, but even the accuracy of its calculation is difficult to assess. Therefore, verification of the calculation results by classical methods is relevant, and in modern conditions this can be done on the basis of numerical methods for calculating magnetic fields by available software complexes and the accompanying harmonic analysis.

3. The absence of such studies is explained by their complexity and significant labor intensity, which is practically impossible to carry out in the «manual» mode. Therefore, to overcome the problems of calculations, an automated software complex was created in the form of a single Lua script, which provides a physically transparent path to the DLR, which runs through the design of the TIM of its physical and geometric model in the FEMM software environment, control of magnetic field calculations, determination of the time functions of the MFL and EMF and their harmonic analysis.

4. Comparison of the results of classical and numerical-field calculations of DLR using the FEMM code showed their large discrepancy, which is attributed to the above-mentioned conventions and assumptions of the first. But the second option is devoid of the shortcomings of the first due to the fact that it takes into account the dimensions of the TIM structures, the saturation of the magnetic core and the physical and mathematical essence of the parameters and quantities under consideration. To exclude the randomness of the assessment, the computational analysis was performed for nine common TIM options, designed using a single classical method with varying their power and number of poles.

5. It was found that the DLR of the TIM stator winding significantly depends on the saturation level of its magnetic system, increasing with increasing saturation of the tooth zone. If we take a completely unsaturated system, then in the stator winding there remains practically only the first harmonic of the EMF, and differential scattering becomes insignificant. The classical method does not focus on this and provides a universal formula for calculating the DLR.

6. The conducted studies have shown that numerical-field calculations of differential parameters of the TIM stator winding are universal, therefore they can be proposed for similar calculations for both the stator and the rotor of various AC electric machines. Moreover, given the software implementation based on the FEMM code and the Lua script, such calculations can be built into automated design methods for these machines.

Conflict of interest. The author declares no conflict of interest.

REFERENCES

1. Goldberg O.D., Gurin Ya.S., Sviridenko I.S. *Design of electrical machines. 2nd ed., revised and additional*. Moscow, Higher School Publ., 2001. 430 p. (Rus).

2. Kopylov I.P., Goryainov F.A., Klokov B.K. *Electrical machines designing*. Moscow, Yurait Publ., 2011. 767 p. (Rus).

3. Udomsuk S., Areerak K., Areerak T., Areerak K. Online Estimation of Three-Phase Induction Motor Parameters Using an Extended Kalman Filter for Energy Saving. *Energies*, 2024, vol. 17, no. 9, art. no. 2115, pp. 1-17. doi: https://doi.org/10.3390/en17092115.

4. Aib A., Khodja D.E., Chakroune S., Rahali H. Fuzzy current analysis-based fault diagnostic of induction motor using hardware co-simulation with field programmable gate array. *Electrical Engineering & Electromechanics*, 2023, no. 6, pp. 3-9. doi: https://doi.org/10.20998/2074-272X.2023.6.01.

5. Abu Ibaid O.Z.I., Belhamdi S., Abid M., Chakroune S., Mouassa S., Al-Sagar Z.S. Wavelet packet analysis for rotor bar breakage in an inverter induction motor. *Electrical Engineering & Electromechanics*, 2023, no. 3, pp. 3-11. doi: https://doi.org/10.20998/2074-272X.2023.3.01.

6. Sakhara S., Brahimi M., Nacib L., Layadi T.M. Application of a wavelet neural network approach to detect stator winding short circuits in asynchronous machines. *Electrical Engineering & Electromechanics*, 2023, no. 3, pp. 21-27. doi: https://doi.org/10.20998/2074-272X.2023.3.03.

7. Popovych O.M., Golovan I.V. Modeling of induction motors in electromechanical systems considering stator iron losses. *Technical Electrodynamics*, 2024, no. 5, pp. 24-29. (Ukr). doi: https://doi.org/10.15407/techned2024.05.024.

8. Tumbek M., Oner Y., Kesler S. Optimal design of induction motor with multi-parameter by FEM method. *2015 9th International Conference on Electrical and Electronics Engineering (ELECO)*, 2015, pp. 1053-1056. doi: https://doi.org/10.1109/ELECO.2015.7394483.

9. Popovych O.M., Golovan I.V. Complex design tools for improvement of electromechanical systems with induction motors. *Technical Electrodynamics*, 2022, no. 2, pp. 52-59. doi: https://doi.org/10.15407/techned2022.02.052.

10. Peresada S.M., Nikonenko Y.O., Kovbasa S.M., Kuznietsov O. Flux observer adaptive to induction motors active rotor

resistance variations. *Technical Electrodynamics*, 2022, no. 5, pp. 45-51. (Ukr). doi: https://doi.org/10.15407/techned2022.05.045.
11. Milykh V.I. Numerical-field analysis of active and reactive winding parameters and mechanical characteristics of a squirrel-cage induction motor. *Electrical Engineering & Electromechanics*, 2023, no. 4, pp. 3-13. doi: https://doi.org/10.20998/2074-272X.2023.4.01.
12. Milykh V. Numerical-field analysis of the magnetic conductivity of the slot dispersion of the stator winding of induction motors. *Bulletin of NTU «KhPI». Series: Problems of electrical machines and apparatus perfection. Theory and practice*, 2023, no. 2 (10), pp. 13-19. (Ukr). doi: https://doi.org/10.20998/2079-3944.2023.2.03.
13. Diarra M.N., Li Y., Zhao X. Induction Motors Parameters Identification by Starting Process Using Quantum Particle Swarm Optimization-Trust Region Algorithm (QPSO-TRA). *2023 International Conference on Applied Intelligence and Sustainable Computing (ICAISC)*, 2023, pp. 1-6. doi: https://doi.org/10.1109/ICAISC58445.2023.10200090.
14. Rajput S., Bender E., Averbukh M. Simplified algorithm for assessment equivalent circuit parameters of induction motors. *IET Electric Power Applications*, 2020, vol. 14, no. 3, pp. 426-432. doi: https://doi.org/10.1049/iet-epa.2019.0822.
15. Lee K., Frank S., Sen P.K., Polese L.G., Alahmad M., Waters C. Estimation of induction motor equivalent circuit parameters from nameplate data. *2012 North American Power Symposium (NAPS)*, 2012, pp. 1-6. doi: https://doi.org/10.1109/NAPS.2012.6336384.
16. Gülbahçe M.O., Karaaslan M.E. Estimation of induction motor equivalent circuit parameters from manufacturer's datasheet by particle swarm optimization algorithm for variable frequency drives. *Electrica*, 2022, vol. 22, no. 1, pp. 16-26. doi: https://doi.org/10.5152/electrica.2021.21122.
17. Mölsä E., Tiitinen L., Saarakkala S., Peretti L., Hinkkanen M. Standstill Self-Commissioning of an Induction Motor Drive. *2020 IEEE Energy Conversion Congress and Exposition (ECCE)*, 2020, pp. 3044-3050. doi: https://doi.org/10.1109/ECCE44975.2020.9236035.
18. Chen H., Bi C. An effective method for determination and characteristic analysis of induction motor parameters. *IET Electric Power Applications*, 2022, vol. 16, no. 5, pp. 605-615. doi: https://doi.org/10.1049/elp2.12180.
19. Caruso M., Tommaso A.O.D., Giangrasso L., Marignetti F., Miceli R., Rizzo R. Differential Leakage Factor in Electrical Machines Equipped with Asymmetrical Multiphase Windings: a General Investigation. *2019 Fourteenth International Conference on Ecological Vehicles and Renewable Energies (EVER)*, 2019, pp. 1-7. doi: https://doi.org/10.1109/EVER.2019.8813617.
20. Di Tommaso A.O., Genduso F., Miceli R., Ricco Galluzzo G. An Exact Method for the Determination of Differential Leakage Factors in Electrical Machines With Non-Symmetrical Windings. *IEEE Transactions on Magnetics*, 2016, vol. 52, no. 9, pp. 1-9. doi: https://doi.org/10.1109/TMAG.2016.2562602.
21. Guedes J.J., Castoldi M.F., Goedtel A., Agulhari C.M., Sanches D.S. Parameters estimation of three-phase induction motors using differential evolution. *Electric Power Systems Research*, 2018, vol. 154, pp. 204-212. doi: https://doi.org/10.1016/j.epsr.2017.08.033.
22. *Slobozhansky Electromechanical Plant «SLEMZ»*. Available at: https://slemz.com.ua (Accessed: 26 August 2024).
23. *DNEPRORESURS LLC*. Available at: https://elmo.ua/uk (Accessed: 26 August 2024).
24. *Finite Element Method Magnetics: Download – Stable Distribution (21Apr2019) – 64-bit Executable.* Available at: https://www.femm.info/wiki/Download (Accessed: 22 July 2024).
25. Milykh V.I. Numerical-field analysis of temporal functions and harmonic composition of EMF in windings of a three-phase asynchronous motor. *Technical Electrodynamics*. 2018, no. 3, pp. 56-65. (Rus). doi: https://doi.org/10.15407/techned2018.03.056.
26. Milykh V.I. The system of automated formation of electrical machines computational models for the FEMM software environment. *Technical Electrodynamics*. 2018, no. 4, pp. 74-78. (Ukr). doi: https://doi.org/10.15407/techned2018.04.074.
27. Milykh V.I., Polyakova N.V. Harmonious analysis of electromagnetic sizes three-phase winding of stators of turbogenerator on basis classic and numeral field methods. *Technical Electrodynamics*, 2013, no. 3, pp. 40-49. (Rus).

Received 02.09.2024
Accepted 05.11.2024
Published 02.03.2025

V.I. Milykh[1], *Doctor of Technical Science, Professor,*
[1] National Technical University «Kharkiv Polytechnic Institute», 2, Kyrpychova Str., Kharkiv, 61002, Ukraine,
e-mail: mvikemkpi@gmail.com

How to cite this article:
Milykh V.I. Numerical-field analysis of differential leakage reactance of stator winding in three-phase induction motors. *Electrical Engineering & Electromechanics*, 2025, no. 2, pp. 7-18. doi: https://doi.org/10.20998/2074-272X.2025.2.02